



Tomographic study of the structure of cast and pressed trotyl charges

N.P. Satonkina^{a,b,*}, K.E. Kuper^{c,d}, A.P. Ershov^a, E.R. Prueel^a, A.S. Yunoshev^a,
Ya.L. Lukyanov^a, D.V. Gusachenko^a, A.S. Khorungenko^b, A.A. Kuzminykh^b

^a Lavrentyev Institute of Hydrodynamics, SB RAS, 630090, Novosibirsk, Russia

^b Novosibirsk State University, 630090, Novosibirsk, Russia

^c Budker Institute of Nuclear Physics, SB RAS, 630090, Novosibirsk, Russia

^d Siberian Branch of the Russian Academy of Sciences, 630090, Novosibirsk, Russia

ARTICLE INFO

Keywords:

TNT
structure
detonation
reaction zone kinetics
electrical conductivity during detonation
sensitivity

ABSTRACT

The sensitivity of condensed explosives depends strongly on the charge structure. Trotyl (TNT) is a typical example of such dependence. The pressed charges are more sensitive than the cast ones, which was confirmed in many studies including critical diameter tests and chemical spike width estimates. Our measurements of the electrical conductivity distributions in the dense TNT support the same conclusion.

In this paper, results of tomographic study of the structure of pressed and cast trotyl are presented. The distribution functions of pores larger than 4 μm were obtained using synchrotron X-raying. In cast TNT, voids varying from units to hundred microns were observed, while the pressed charge was found to be substantially more uniform and less porous. The roles of possible mechanisms of hot spots generation are discussed.

1. Introduction

The reaction kinetics, as well as the critical parameters of the energetic materials, are sensitive to the charge structure. According to the generally accepted understanding, the reaction starts within the multiple local non-uniformities, usually called hot spots [1–14].

Among the various mechanisms capable to generate hot spots under shock impact, collapse of pores is regarded as one of the most probable scenarios [3–6]. In a number of papers, such collapse is treated numerically, usually starting from geometrically regular voids. In order to understand the physics of the collapse, experimental and numerical study of void deformation in an inert material (PMMA) were performed for different amplitudes of shocks – from weak ones to those typical for detonation waves [15]. In the work [7], reaction in voids in TATB (tri-aminotrinitrobenzene) and HMX (cyclotetramethylenetetranitramine) was modeled at different shock pressures P_5 . The dependence of critical pore size on P_5 was obtained. At the typical detonation pressures, voids of less than 0.5 μm in diameter became effective. For TATB, the highest temperatures (1 500–1 800 K) are reached in collapse of small pores. The maximal size of voids in simulations was about 4 μm .

In several papers, the effect of the morphology and arrangement of voids on the sensitivity was studied [8–10]. Shock impact on the powdered HMX using real size distribution of grains was simulated

[16–18].

Other non-uniformities can be considered as hot spot precursors as well. A review of the influence of the crystal defects on the sensitivity of the energetic materials is presented in the work [11]. In work [12], structural non-uniformities are considered which can lead to ignition under shock waves. In the work [13], shocks in TATB were modeled using molecular dynamics. Nanometer-scaled shear bands were found in which the reaction barrier was somewhat lower, which should favor the ignition. In the work [14], to describe the initiation of the explosive, a multiscale model is proposed incorporating the range from molecular level to macroscale, taking the material structure into account. Other multiscale models are considered in works [4,6].

Given the progress in computational power, the modeling becomes more detailed, with increased resolution and new physical effects incorporated into codes. But, without the actual structure parameters, the capacity of the numerical simulations is obviously limited.

The variability of the critical diameter d_{cr} observed for the charges prepared using different procedures is a clear illustration of the sensitivity-structure relationship. For TNT, this phenomenon is quite pronounced. In Table I, critical diameters for dense TNT of various structures are presented. Even for the similar technology (cast charges) d_{cr} can differ by the factor 2 (lines 4, 5 and 6, 7, 9), and for higher density the critical diameter is smaller. Largest critical diameters were found in

* Corresponding author. Lavrentyev Institute of Hydrodynamics, SB RAS, 630090, Novosibirsk, Russia.

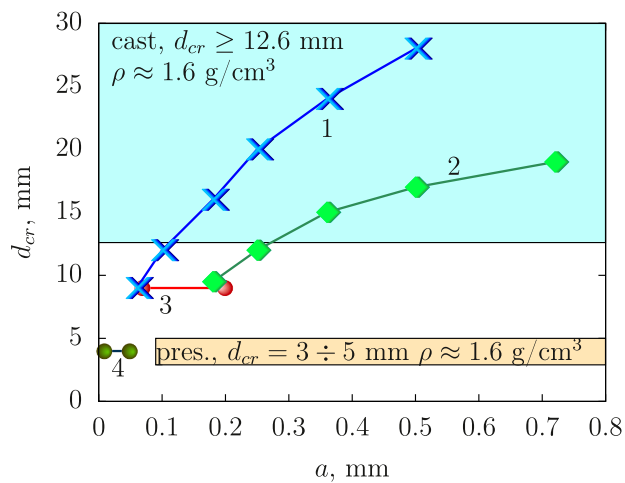
E-mail address: snp@hydro.nsc.ru (N.P. Satonkina).

<https://doi.org/10.1016/j.rineng.2022.100621>

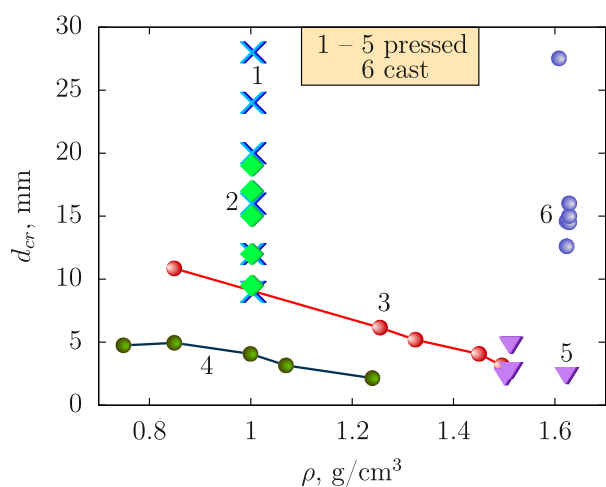
Received 7 July 2022; Received in revised form 28 August 2022; Accepted 29 August 2022

Available online 9 September 2022

2590-1230/© 2022 The Author(s). Published by Elsevier B.V. This is an open access article under the CC BY license (<http://creativecommons.org/licenses/by/4.0/>).



(a)



(b)

Fig. 1. (a) Critical diameter of TNT with different grain size and structure, curves 1, 2, 3, 4 corresponding to the density of 1 g/cm³. 1 – crushed fractionated TNT of a homogeneous structure [24,25], 2 – aggregate fractionated [25], 3, 4 – the charge is placed in a thin-walled glass tube, the horizontal lines show the dispersion range [20]. Color-filled areas show the range of values at close to maximum density for pressed and cast charges. (b) Dependence of critical diameter on density: 1, 2 – at different dispersity (data correspond to Fig. 1(a)), 3 and 4 – charge with different initial grain size is in a thin-walled glass tube [20], 5 – pressed high-density charge, 6 – cast charge, data of Table 1.

monocrystal and in liquid TNT.

The dependence of the TNT critical diameter at the bulk density of 1 g/cm³ on grain size *a* is shown in Fig. 1(a). 1: grains are solid, 2: grains are aggregates (powdered TNT with 0.06 mm particle size was pressed to 1.5 g/cm³, then crushed and fractionated), 3, 4: powdered TNT of different grain size, the charges fill thin glass tube. The coloured areas mark the critical diameters for dense cast and pressed TNT. The critical diameter at fixed density is smaller for small grain size. When *a* increases, *d_{cr}* falls into the area of dense insensitive cast TNT.

The dependence of the critical diameter on density is shown in Fig. 1 (b) for all data except monocrystal and liquid state. At the similar density *d_{cr}* differs for an order of magnitude in cast and pressed charges (Table 1, lines 4, 5 and 8). The range of *d_{cr}* values is the same, both at bulk density and at the maximal one, so it is not possible to relate the sensitivity to the density. The data in Table 1 and Fig. 1 suggest that

Table 1

Critical diameter *d_{cr}* of TNT charge at the different manufacturing methods.

| N | Method of making a charge | ρ , g/cm ³ | <i>d_{cr}</i> , mm | ref. |
|-----|-------------------------------------|----------------------------|----------------------------|----------|
| 1. | liquid | 1.443 | 62.6 ± 2.6 | [19] |
| 2. | pressed in a thin-walled glass tube | 1.50 | 2.5 | [20] |
| 3. | pressed | 1.51 | 3 ÷ 5 | [19] |
| 4. | cast type II ^a | 1.60 | 27.5 | [21] |
| 5. | cast “coarse-crystal” ^a | 1.60 | 27.5 | [22] |
| 6. | creaming and casting | 1.615 | 14.6 ± 2.0 | [19] |
| 7. | layer-by-layer casting | 1.615 | 12.6 | our data |
| 8. | pressed | 1.62 | 2.6 ± 0.6 | [19] |
| 9. | vacuum melting and casting | 1.62 | 14.5 ± 0.5 | [19] |
| 10. | cast “fine crystal” ^a | 1.62 | 15 | [22] |
| 11. | cast type I ^a | 1.62 | 16 | [21] |
| 12. | single crystal | 1.663 | 110 | [23] |

^a Retained original name.

neither density, nor grain size or porosity, taken separately, are key factors for sensitivity. The decisive factor is the charge structure. Thus, detailed study of the charge structure is necessary to understand which nonuniformities, of which type and scale, affect the sensitivity.

Theoretical attempts to derive the pore space configuration from the initial grain size are hardly practical [20,26]. One can observe the charge surface, but its morphology is likely different from that inside the charge. The surface of the sliced or cracked specimen is also distorted (as one can see from the data presented below). For the cast TNT, the morphology of the voids depends on casting technology, the cooling rate, charge geometry, casing material, etc. and is even more uncertain. The properties of cast TNT are so sensitive to the subtle details of technology, that such details are accurately described for each charge sort [21,22,27]. So, the scanning of real inner structure of explosive is an actual and interesting problem.

This paper offers a non-destructive method to study an actual three-dimensional charge structure.

2. Experiment

2.1. Charge preparation

For the pressed charge, commercial TNT was used. Original flakes were crushed manually in a ceramic mortar. The images of grains are shown in Fig. 2. The main part of the explosive grains had the size of 10–30 μm. TNT was pressed at about 90 atm. The density was $\rho_{pres} = 1.6198 \pm 0.0099$ g/cm³, the corresponding porosity was 0.0260.

The density of liquid TNT ($\rho_{liquid} = 1.467$ g/cm³) is lower than that of solid material ($\rho_{crystal} = 1.663$ g/cm³) [28], which is a main source of defects in cast charges. To minimize the forming of large inner voids, the cast charges were prepared pouring multiple thin layers. The density of cast charge was $\rho_{cast} = 1.6151 \pm 0.0029$ g/cm³, the corresponding porosity was $m_{cast,exp} = 0.0288$.

The samples used for tomography were cylinders with a diameter of 1.5 mm, which were cut from larger pellets.

2.2. Tomography method

Numerical X-ray tomography provides three-dimensional data describing the structure of specimens under study. The data can be represented as a stack of coloured density maps. White areas will mean the maximal density. The pores have contrast boundaries which allows one to get their clear distribution.

The sketch of the measuring facility is presented in Fig. 3. The X-ray source was synchrotron radiation (SR) beam produced by wiggler incorporated into VEPP-3 accelerator (Institute of Nuclear Physics, RAS Siberian Branch). The angular spread VEPP-3 SR beam is 0.1 milliradian, and total beam X-ray power is 100 W. The small angular dispersion and high brightness of SR allows one to obtain good spatial resolution, about 2 μm for short-wave range (5–30 keV), used for explosive diagnostics.

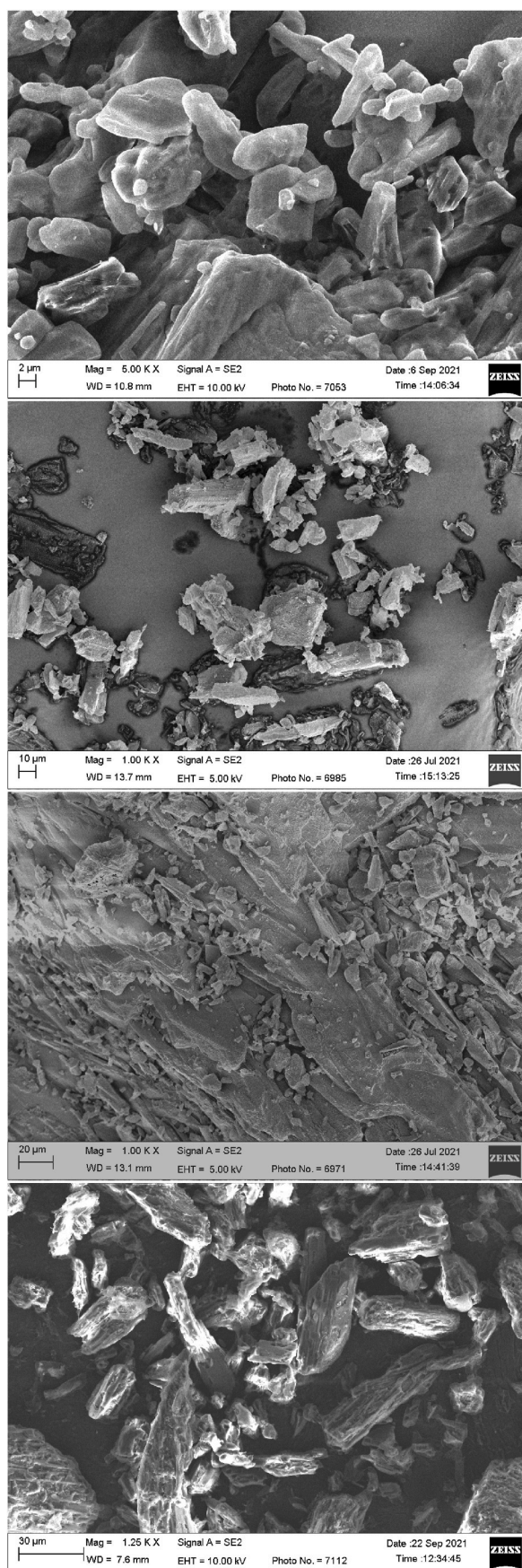


Fig. 2. Micrographs of the initial grains used in pressing.

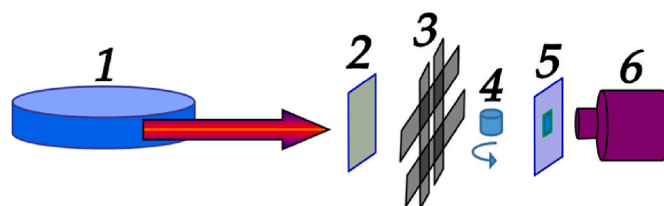


Fig. 3. Diagram of a tomographic study of the chargedensity: 1 - source of synchrotron radiation VEPP-3, 2 - filter, 3 - collimator, 4 - sample on a rotating stand, 5 - scintillator, 6 - detector.

Aluminium was chosen as a material for X-ray filters since it does not have any peculiarities in the used energy range. The absorption of explosive specimens was recorded using thin scintillation screen. The main sensing material was cesium iodide doped by tellurium CsI(Tl), which has high luminous yield and is effective in X-ray range. A high-resolution CCD array (Hamamatsu ORCA-Flah2.8) with a size of 2048×2048 pixels was used as a detector. Single pixel size, taking objective magnification factor into account, was $0.6 \mu\text{m}$. The dynamic intensity range of the detector was 16 bit. The specimen, scintillation screen and detector were positioned with $1 \mu\text{m}$ linear and 0.001 angular accuracy. To form the SR beam, $1.5 \times 1.5 \text{ mm}$ X-ray collimator was used.

The specimen was rotated, and a set of the projections was recorded, which was used to restore three-dimensional map [29,30]. The final spatial resolution was $2.6 \mu\text{m}$.

3. Tomographic study of cast and pressed TNT: results

In Fig. 4, an example of tomographic data is presented (multimedia view contained in Supplementary data). Two cross-sections picked from the inner parts of charges correspond to cast and pressed TNT. Cast charge is highly nonuniform. One can see multiple pores up to dozens of μm in size. Some voids (marked by circles) have surfaces of concave form. The pressed specimen is more uniform, pores are generally smaller, though large pores are present in fewer number.

In Fig. 5, the tomographic sections are compared with the initial TNT grains. On the cut of the pressed charge, cracks are visible, which were formed during manipulations with the sample in the process of manufacturing and processing to the desired shape. The cavities are predominantly compact in shape, close to ideal, although there are also pores with a concave inner surface. No traces of grains can be identified in the pressed specimen. Since TNT is not very strong material, the grains are easily deformed under pressing, which leads to better uniformity and to smoothing of the boundaries of grains. The cracks visible in the pressed charge arise presumably during the extracting of the specimen from the mold.

The initial data of the tomographic examination and layer-by-layer visualization can be found at the link <http://ancient.hydro.nsc.ru/tomography>.

3.1. Statistic of voids

For comparative analysis, from the numerical specimens obtained by X-raying the cast and pressed TNT, two identical cylinders were cut containing 600 cells in diameter and 451 cells high. The cell size was $2.6 \mu\text{m}$, and the total physical volume $V_0 \approx 2.24 \text{ mm}^3$. Fig. 6 displays the distributions of pore numbers $N_p(d)$, volume of voids $V_p(d)$ and surface of voids $S_p(d)$ on d at Fig. 7(a). Here, d is the diameter of sphere which has the volume equal to the pore volume. For all graphs, general decrease with increasing d is observed. Maximal values correspond to the minimal displayed $d = 4 \mu\text{m}$. For this size, pore numbers, pore volumes and pore surface for cast and pressed specimen do not differ significantly. However, the cast charge clearly has more large pores. In the cast charge, voids which have $d > 10 \mu\text{m}$ are present in significant

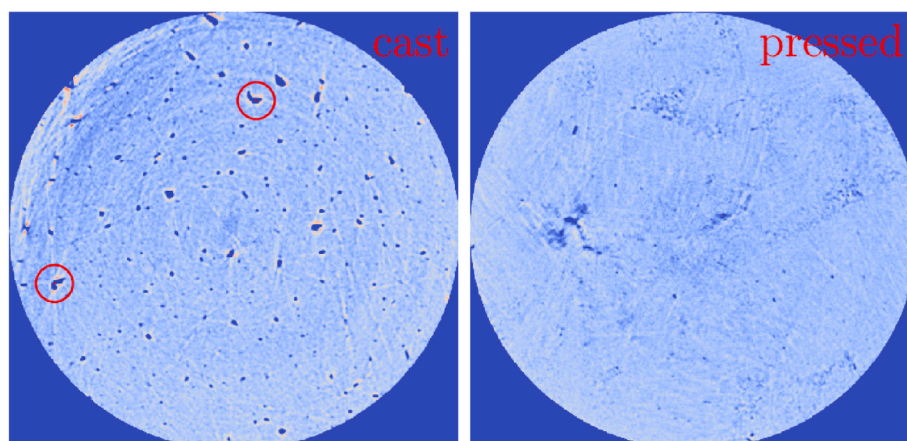


Fig. 4. Structure of charge. Sample diameter 1.5 mm, cast on the left, pressed on the right. The cast contains pores with a concave inner surface (highlighted by circles). The shape of the pores is represented by various geometrically irregular figures.

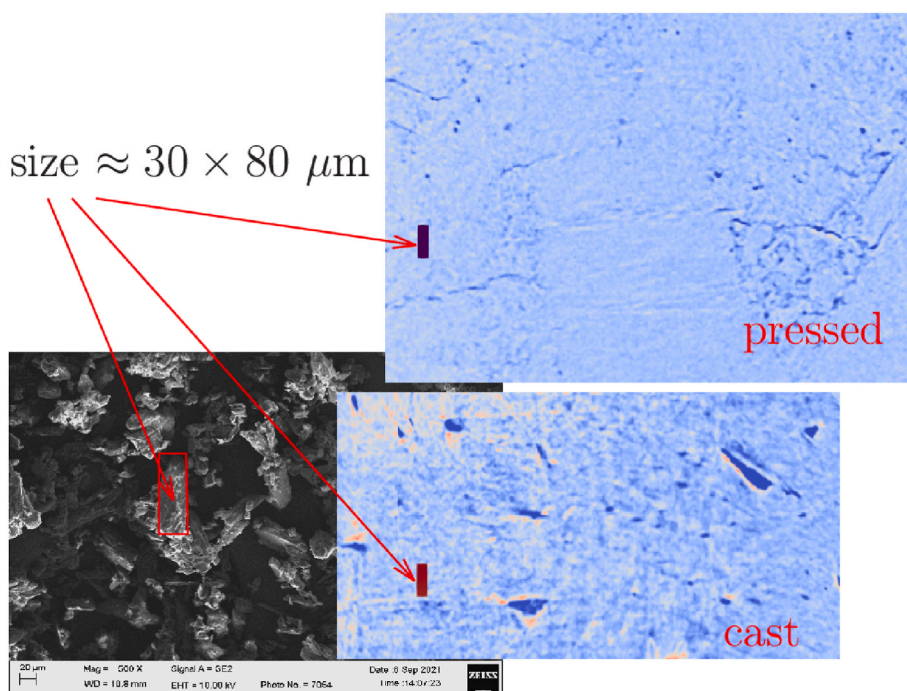


Fig. 5. Tomographic sections and a microphotograph of crushed explosive grains are shown; all photos show a $30 \times 80 \mu\text{m}$ fragment.

number, their volume is about 10% of total pore space. The equivalent diameter of largest pores in cast charge is $\approx 70 \mu\text{m}$ while in the pressed charge the corresponding value is $\approx 20 \mu\text{m}$.

The largest pores found in cast TNT can be fragmented behind the shock wave, forming several smaller pores. Each fragment can generate hot spot. Thus, large irregular pores potentially may be not less effective for ignition than smaller ones.

Fig. 7(b) shows the integral volume of pores calculated from minimal resolved size to the given d value. The results of the tomographic study are in good agreement with the data of direct density measurements. Some difference within error margins may occur due to limited spatial resolution (e.g., pores smaller than $4 \mu\text{m}$ are ignored) or from computational errors arising for highly irregular large pores. This problem will be addressed in the following study. For now, the tomographic method seems to be more perspective than common approaches such as observation from surface or percolation experiments [31].

Note that the tomographic method for studying the internal structure of objects finds wide practical application in medicine [32–37], for

geological exploration using a probe beam with different wavelengths, the method is suitable for studying structures of various and material properties, see Ref. [38] for example. In this work, the method of tomographic research is used in relation to explosives.

4. Electrical conductivity distribution

Previously, we developed a technique to measure electrical conductivity profile behind the detonation wave front in dense high explosives [39,40]. The consistency between the conductivity and the carbon content was confirmed [41–44]. For RDX (cyclotrimethylene trinitramine) [45], HMX, PETN (pentaerythritol tetranitrate) [40], BTF (benzotrifuroxan) [46], TATB [47], HNS (hexanitrostilbene) and TNT [48], the conductivity was found to increase with the density [49–51]. The correlation of the conductivity peaks and the chemical reaction zone was established [52–54]. This opens a perspective to use the conductivity diagnostics to study the chemical reaction kinetics in detonation waves.

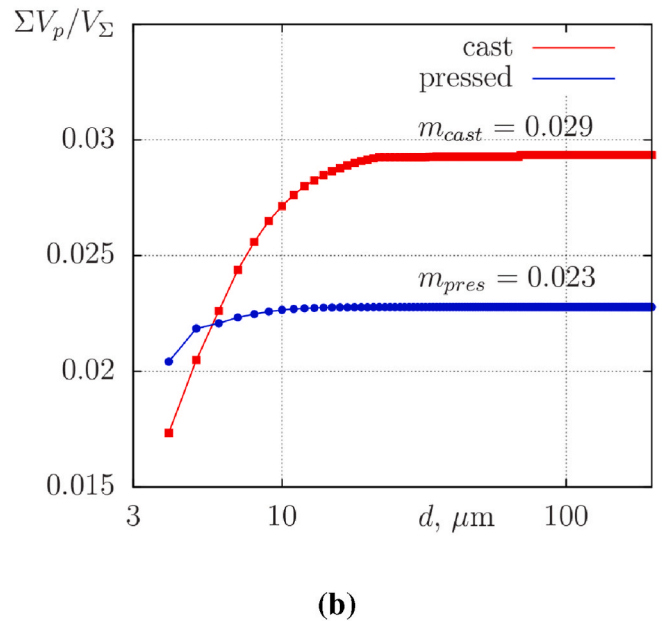
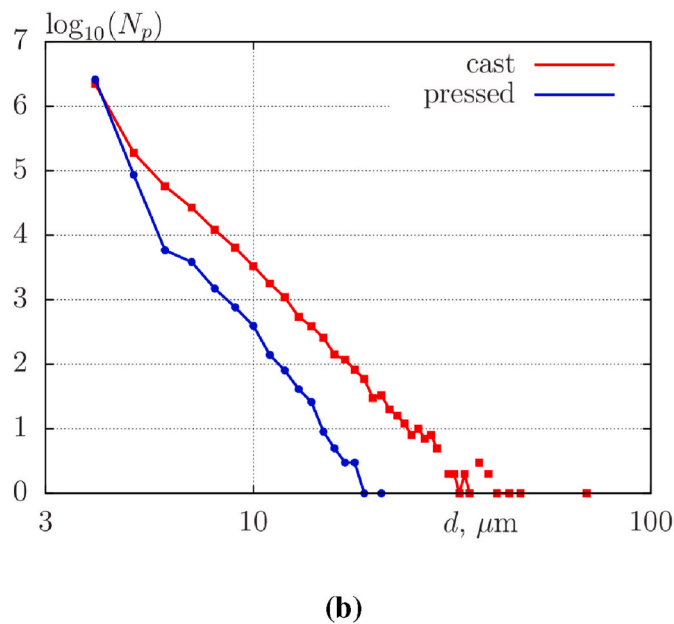
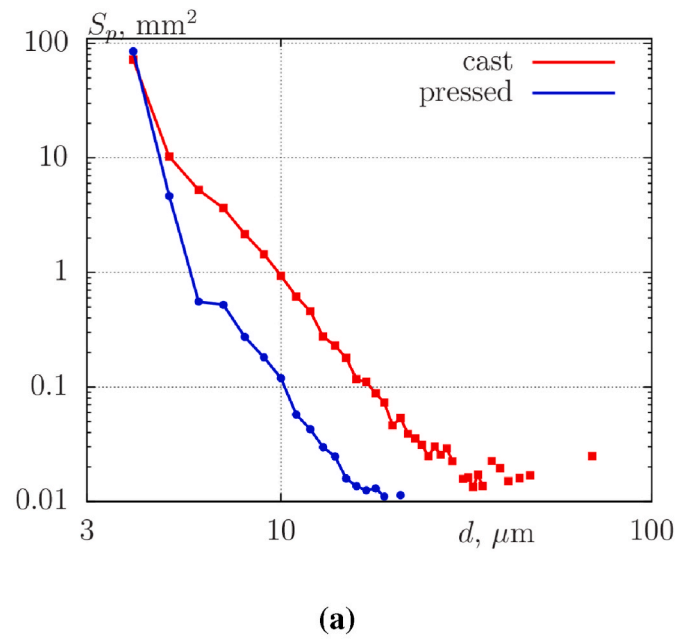
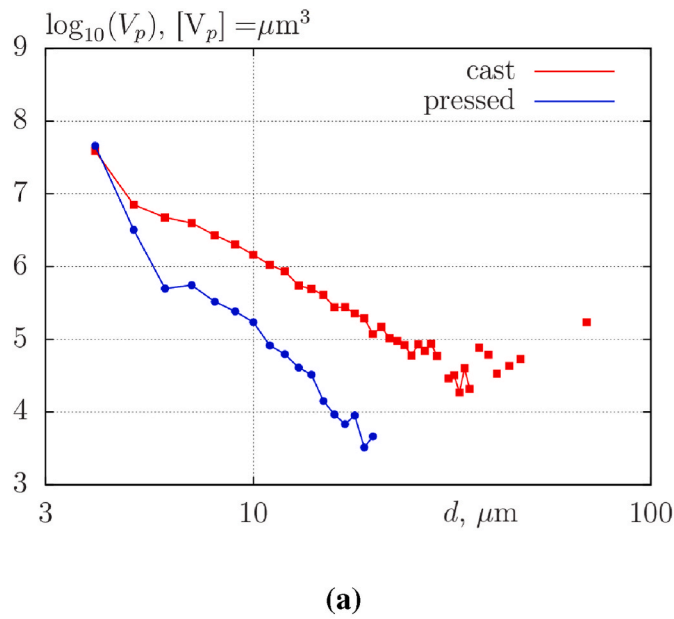


Fig. 6. The results of a tomographic study of voids in a cast and pressed charge: (a) – volume of pores V_p for a standard spherical pore diameter d , (b) – number of pores N_p .

In Fig. 8 electrical conductivity profiles in detonating TNT are shown: pressed (curve 1) and cast (curve 2). The experiments were performed using the same procedure as in works [39,40]. Both cast and pressed charges were prepared in a manner similar to that described in Sec. 2. The detonation velocities (see Fig. 8) are almost equal. Nevertheless, the conductivity profiles are quite different. To our opinion, sharp triangular peak ($\sigma_{max} \approx 100 \text{ Ohm}^{-1}\text{cm}^{-1}$) in pressed TNT indicates higher reaction rate whereas in cast charge the conductivity is four times lower, and the reaction is slower. The high value of electrical conductivity, similar to that obtained for pressed TNT, is confirmed by the results of the works [55,56]. It is well known that the sensitivity of the pressed TNT charge is higher than that of the pressed one, this is true for both the critical diameter and the shock wave sensitivity [57–62]. Our interpretation of the electrical conductivity data on different chemical reaction rates is in good agreement with the known information on critical diameters. According to Kobylkin [63–65], critical

Fig. 7. The results of a tomographic study of voids in a cast and pressed charge: (a) – inner surface area S_p , $S_{p,pres} = 244 \text{ cm}^2/\text{g}$, $S_{p,cast} = 273 \text{ cm}^2/\text{g}$, (b) – integral over pores normalized to the sample volume. Porosity m_{cast} and m_{pres} calculated from tomographic data.

diameter is in inverse proportion to the reaction rate. The fact that the critical diameter of pressed TNT is smaller than that in cast trotyl means that in pressed explosive, the reaction rate is higher. The results of papers [60,61], which reported about five times higher reaction rate in pressed TNT ($\rho = 1.56 \text{ g/cm}^3$) as compared with cast TNT ($\rho = 1.61 \text{ g/cm}^3$) also support this view.

5. Conclusion

Sharp difference in the reaction rates of pressed and cast TNT charges is a well established fact. In the preceding sections we mentioned indicators of this difference, including critical diameter data, direct measurements of the pressure profile, and added a comparison of the electrical conductivity distributions. All evidence is in favor of the

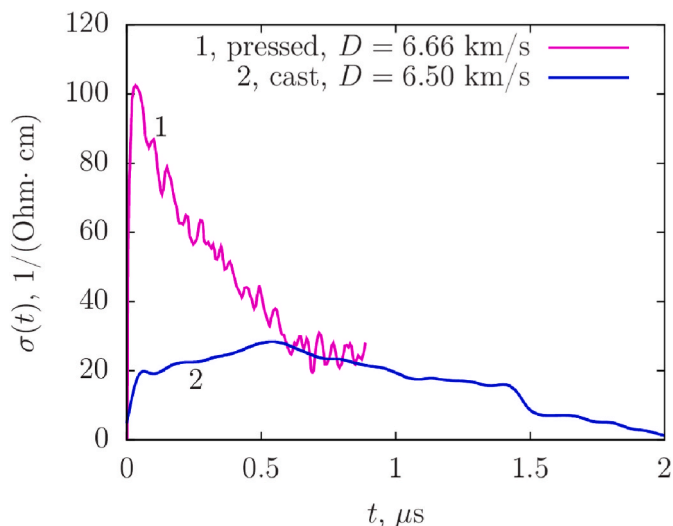


Fig. 8. Electrical conductivity profiles in detonating TNT: 1 – pressed [49], 2 – cast.

conclusion that pressed TNT is more active explosive.

Nevertheless, our tomographic data seem to contradict this conclusion. While the number of smallest resolvable pores ($d \approx 4 \mu\text{m}$) was almost equal, the larger voids in cast charge were sufficiently more numerous than in the pressed one. However, the pores are regarded as most probable precursors of the hot spots.

To our opinion, this contradiction can be resolved in two alternative ways. Either collapse of pores is actually the working process, but the active voids are smaller than $4 \mu\text{m}$, and our spatial resolution was insufficient to observe them. According to different view, not pores but multiple contact boundaries between the explosive grains are the main source of hot spots in the pressed charge. The molecules which form the boundaries are in different state than those inside the microcrystals, their activation energy can be lower, and deformation effect in such locations should be more intense. Thus, the grain boundaries seem to be perspective as the ignition sites. These conclusions are in good agreement with the work [66] in which an alternative for pore collapse kinetics is proposed, based on the diagnosis of a chemical reaction zone through electrical conductivity. For now, the mechanism of void collapse seems to be more popular in the literature. But it may be rather the result of more clear physical picture and more convenient numerical modeling of this process, than of solid justification needed for an established theory.

To our information, the tomographic study is coupled with the sensitivity data for the first time in the present paper.

Declaration of competing interest

The authors declare that they have no known competing financial interests or personal relationships that could have appeared to influence the work reported in this paper.

Acknowledgments

This research was funded by the Ministry of Science and Higher Education of the Russian Federation (project N 075-15-2020-781).

Appendix A. Supplementary data

Supplementary data to this article can be found online at <https://doi.org/10.1016/j.rineng.2022.100621>.

References

- [1] B.A. Khasainov, A.V. Attekov, A.A. Borisov, Shock-wave initiation of porous energetic materials and visco-plastic model of hot spots, *Chem. Phys. Rep.* 15 (7) (1996) 987–1062.
- [2] C.A. Handley, B.D. Lambourn, N.J. Whitworth, H.R. James, W.J. Belfield, Understanding the shock and detonation response of high explosives at the continuum and meso scales, *Appl. Phys. Rev.* 5 (1) (2018), 011303.
- [3] N.K. Bourne, A.M. Milne, The temperature of a shock-collapsed cavity, *Proc. Roy. Soc. Lond. A* 459 (2036) (2003) 1851–1861.
- [4] M.A. Wood, D.E. Kittell, C.D. Yarrington, A.P. Thompson, Multiscale modeling of shock wave localization in porous energetic material, *Phys. Rev. B* 97 (1) (2018), 014109, <https://doi.org/10.1103/PhysRevB.97.014109>.
- [5] E.M. Escariza, J.P. Duarte, D.J. Chapman, M.E. Rutherford, L. Farbaniec, J. C. Jonsson, L.C. Smith, M.P. Olbinado, J. Skidmore, P. Foster, T. Ringrose, A. Rack, D.E. Eakins, Collapse dynamics of spherical cavities in a solid under shock loading, *Sci. Rep.* 10 (1) (2020) 8455.
- [6] M.P. Kroonblawd, R.A. Austin, Sensitivity of pore collapse heating to the melting temperature and shear viscosity of HMX, *Mech. Mater.* 152 (2021), 103644.
- [7] N.K. Rai, O. Sen, H.S. Udaykumar, Macro-scale sensitivity through meso-scale hotspot dynamics in porous energetic materials: comparing the shock response of 1,3,5-triamino-2,4,6-trinitrobenzene (TATB) and 1,3,5,7-tetranitro-1,3,5,7-tetra-zoctane (HMX), *J. Appl. Phys.* 128 (8) (2020), 085903.
- [8] R.A. Austin, N.R. Barton, W.M. Howard, L.E. Fried, Modeling pore collapse and chemical reactions in shock-loaded HMX crystals, *J. Phys. Conf. Ser.* 500 (PART 5) (2014), 052002.
- [9] H.K. Springer, S. Bastea, I.I.I. Nichols, L. A. C.M. Tarver, J.E. Reaugh, Modeling the effects of shock pressure and pore morphology on hot spot mechanisms in HMX, *Propellants, Explos. Pyrotech.* 43 (8) (2018) 805–817.
- [10] C. Li, B.W. Hamilton, A. Strachan, Hotspot formation due to shock-induced pore collapse in 1,3,5,7-tetranitro-1,3,5,7-tetra-zoctane (HMX): role of pore shape and shock strength in collapse mechanism and temperature, *J. Appl. Phys.* 127 (17) (2020), 175902.
- [11] K. Zhong, R. Bu, F. Jiao, G. Liu, C. Zhang, Toward the defect engineering of energetic materials: a review of the effect of crystal defects on the sensitivity, *Chem. Eng. J.* 429 (2022), 132310.
- [12] V.S. Solov'ev, Some specific features of shock-wave initiation of explosives, *Combust. Explos. Shock Waves* 36 (6) (2000) 734–744.
- [13] M.P. Kroonblawd, L.E. Fried, High explosive ignition through chemically activated nanoscale shear bands, *Phys. Rev. Lett.* 124 (20) (2020), 206002.
- [14] P. Das, P. Zhao, D. Perera, T. Sewell, H.S. Udaykumar, Molecular dynamics-guided material model for the simulation of shock-induced pore collapse in β -octahydro-1,3,5,7-tetranitro-1,3,5,7-tetrazocine (β -HMX), *J. Appl. Phys.* 130 (8) (2021), 085901.
- [15] N.K. Rai, E.M. Escariza, D.E. Eakins, H.S. Udaykumar, Mechanics of shock induced pore collapse in poly(methyl methacrylate) (PMMA): comparison of simulations and experiments, *J. Mech. Phys. Solid.* 143 (2020), 104075.
- [16] D.J. Benson, P. Conley, Eulerian finite-element simulations of experimentally acquired HMX microstructures, *Model. Simulat. Mater. Sci. Eng.* 7 (3) (1999) 333–354.
- [17] M.R. Baer, Modeling heterogeneous energetic materials at the mesoscale, *Thermochim. Acta* 384 (1–2) (2002) 351–367.
- [18] S. Roy, O. Sen, N.K. Rai, M. Moon, E. Welle, C. Molek, K.K. Choi, H.S. Udaykumar, Structure–property–performance linkages for heterogenous energetic materials through multi-scale modeling, *Multiscale Multidiscip. Model., Exp. Des.* 3 (4) (2020) 265–293.
- [19] T.R. Gibbs, A. Popolato, J.F. Baytos (Eds.), *LASL Explosive Property Data*, 4, University of California Press, 1980, p. 471.
- [20] V.K. Bobolev, Detonation ability and sensitivity of explosives. Institute of chemical physics of the USSR academy of sciences, in: *The Book "Detonation of Condensed and Gas Systems"*. [Detonatsionnaya Sposobnost' I Chuvstvitel'nost' Vzryvchatykh Veshchestv. Dissertatsiya Na Soiskaniye Uchenoy Stepeni Kandidata Khimicheskikh Nauk. V Knige "Detonatsiya Kondensirovannykh I Gazovykh Sistem"], Izd-vo Nauka, Moskva, 1947, p. 320 [In Russian].
- [21] A.N. Dremin, S.D. Savrov, V.S. Trofimov, K.K. Shvedov, *Detonation Waves in Condensed Media [Detonatsionnyye Volny V Kondensirovannykh Sredakh]*, Izd-vo Nauka, Moskva, 1970, p. 164 [In Russian].
- [22] V.V. Kravtsov, V.V. Sil'vestrov, Effect of low temperature on detonation parameters of cast trityl, *Combust. Explos. Shock Waves* 15 (1979) 387–390.
- [23] A.Y. Apin, N.F. Velina, On critical detonation diameters of single crystals of explosives [o kriticheskikh diametrakh detonatsii monokristallov vzryvchatykh veshchestv], *Explosive Detonation and Blasting Safety [Detonatsiya vzryvchatykh veshchestv i bezopasnost' vzryvnykh rabot]* 63/246 (1967) 317–318 [In Russian].
- [24] A.Y. Apin, Influence of physical structure and aggregate state on detonability of high explosives, *Dokl. Akad. Nauk SSSR* 50 (1945) 285–289.
- [25] A.Y. Apin, L.N. Stesik, Critical Diameters of Powdered High Explosives. *Physics of Explosion [Fizika Vzryva]* Sbornik No 3, Izd-vo AN SSSR, 1955, pp. 87–92 [In Russian].
- [26] B.A. Khasainov, B.S. Ermolaev, H.-N. Presles, P. Vidal, On the effect of grain size on shock sensitivity of heterogeneous high explosives, *Shock Waves* 7 (2) (1997) 89–105.
- [27] B.G. Loboiko, S.N. Lubyatinsky, Reaction zones of detonating solid explosives, *Combust. Explos. Shock Waves* 36 (2000) 716–733.
- [28] E.Yu Orlova, *Chemistry and Technology of High Explosives [Kimiya I Tekhnologiya Brizantnykh Vzryvchatykh Veshchestv]*, 395, Oborongiz. Moscow, 1960 [In Russian].

- [29] G.T. Herman, Image Reconstruction from Projections. Fundamentals of Computerized Tomography, Department of Computer Science, State University of New York at Buffalo, 1980, p. 300.
- [30] G.T. Herman, Fundamentals of Computerized Tomography: Image Reconstruction from Projections, Advances in Computer Vision and Pattern Recognition, Springer, London, 2009.
- [31] A.F. Belyaev, V.K. Bobolev, A.I. Korotkov, A.A. Sulimov, S.V. Chuiko, Transition of Combustion of Condensed Systems to Explosion [Perekhod Goreniya Kondensirovannykh Sistem Vo Vzryv], Izd-vo Nauka, Moskva, 1973, p. 292.
- [32] G.T. Herman, Correction for beam hardening in computed tomography, Phys. Med. Biol. 24 (1) (1979) 81–106.
- [33] J. Teuwen, N. Moriakov, C. Fedon, M. Caballo, I. Reiser, P. Bakic, E. García, O. Diaz, K. Michielsen, I. Sechopoulos, Deep learning reconstruction of digital breast tomosynthesis images for accurate breast density and patient-specific radiation dose estimation, Med. Image Anal. 71 (2021), 102061.
- [34] X. Li, Y. Zhang, S. Mao, J. Zhu, Y. Ye, Implementation of a framelet-based spectral reconstruction for multi-slice spiral CT, Front. Physiol. 94 (2021), 682152.
- [35] V. Haase, K. Hahn, H. Schönhuber, K. Stierstorfer, A. Maier, F. Noo, Single-material beam hardening correction via an analytical energy response model for diagnostic CT, Med. Phys. 49 (8) (2022) 5014–5037.
- [36] M. Nakao, M. Hayata, S. Ozawa, H. Miura, K. Yamada, D. Kawahara, K. Miki, T. Nakashima, Yu Ochi, S. Tsuda, M. Seido, Yo Morimoto, Stoichiometric CT number calibration using three-parameter fit model for ion therapy, Phys. Med. 99 (2022) 22–30.
- [37] C. Martinez, J. Fessler, M. Desco, M. Abella, Simple beam hardening correction method (2DCalBH) based on 2D linearization, Phys. Med. Biol. 67 (117) (2022), 115005.
- [38] Apaydin Orhan, Turgay İşseven, Yiğit Çıtır, Selçuk Paker, Işın Erer, Nedim Gökhan Aydın, Extracting tomographic images of interior structures of cylindrical objects and trees using Ground Penetrating Radar method, Result. Eng. 14 (2022), 100410.
- [39] A.P. Ershov, N.P. Satonkina, G.M. Ivanov, High-resolution conductivity profile measurements in detonating pressed explosive, Tech. Phys. Lett. 30 (12) (2004) 1048–1050.
- [40] A.P. Ershov, N.P. Satonkina, G.M. Ivanov, Electroconductivity profiles in dense high explosives, Russ. J. Phys. Chem. (Engl. Transl.) B 1 (6) (2007) 588–599.
- [41] N.P. Satonkina, The dynamics of carbon nanostructures at detonation of condensed high explosives, J. Appl. Phys. 118 (24) (2015), 245901.
- [42] N.P. Satonkina, Correlation of electrical conductivity in the detonation of condensed explosives with their carbon content, Combust. Explos. Shock Waves 52 (4) (2016) 488–492.
- [43] N.P. Satonkina, Chemical composition of detonation products of condensed explosives and its relationship to electrical conductivity, J. Phys.: Conf. Ser. 946 (1) (2018), 012059.
- [44] N.P. Satonkina, A.P. Ershov, A.O. Kashkarov, I.A. Rubtsov, Elongated conductive structures in detonation soot of high explosives, RSC Adv. 10 (30) (2020) 17620–17626.
- [45] N.P. Satonkina, Influence of the grain size of high explosives on the duration of a high conductivity zone at the detonation, Sci. Rep. 9 (1) (2019), 12256.
- [46] N. Satonkina, A. Ershov, A. Kashkarov, A. Mikhaylov, E. Prueel, I. Rubtsov, I. Spirin, V. Titova, Electrical conductivity distribution in detonating benzotrifuroxane, Sci. Rep. 8 (1) (2018) 9635.
- [47] N.P. Satonkina, I.A. Rubtsov, Electrical conductivity distribution during detonation of a TATB-based explosive, Tech. Phys. 61 (2016) 142–145.
- [48] A.P. Ershov, N.P. Satonkina, O.A. Dibirov, S.V. Tsykin, YuV. Yanilkin, A study of the interaction between the components of heterogeneous explosives by the electrical-conductivity method, Combust. Explos. Shock Waves 36 (5) (2000) 639–649.
- [49] A.P. Ershov, N.P. Satonkina, Investigation of the reaction zone in heterogeneous explosives substances using an electrical conductivity method, Combust. Explos. Shock Waves 45 (2) (2009) 205–210.
- [50] N.P. Satonkina, A.A. Safonov, Electrical properties of TNT detonation products, J. Eng. Thermophys. 18 (2) (2009) 177–181.
- [51] N.P. Satonkina, D.A. Medvedev, On the mechanism of carbon nanostructures formation at reaction of organic compounds at high pressure and temperature, AIP Adv. 7 (8) (2017), 085101.
- [52] A.P. Ershov, N.P. Satonkina, Electrical conductivity distributions in detonating low-density explosives — grain size effect, Combust. Flame 157 (5) (2010) 1022–1026.
- [53] A.P. Ershov, A.O. Kashkarov, E.R. Prueel, N.P. Satonkina, V.V. Sil'vestrov, A. S. Yunoshev, A.V. Platinin, Nonideal detonation regimes in low density explosives, J. Appl. Phys. 119 (7) (2016), 075903.
- [54] A.P. Ershov, N.P. Satonkina, A.V. Platinin, A.S. Yunoshev, Diagnostics of the chemical reaction zone in detonation of solid explosives, Combust. Explos. Shock Waves 56 (6) (2020) 705–715.
- [55] B. Hayes, Electrical measurements in reaction zones of high explosives, Symposium (International) on Combustion 10 (1) (1965) 869–874.
- [56] S.D. Gilev, A.M. Trubachev, High electrical conductivity of trotyl detonation products, Tech. Phys. 46 (9) (2001) 1185–1189.
- [57] A. Sollier, P. Hébert, R. Letremy, Chemical reaction zone measurements in pressed trinitrotoluene (TNT) and comparison with triaminotrinitrobenzene (TATB), J. Appl. Phys. 131 (2022), 055902.
- [58] E.L. Lee, C.M. Tarver, Phenomenological model of shock initiation in heterogeneous explosives, Phys. Fluids 23 (12) (1980) 2362–2372.
- [59] A.W. Campbell, W.C. Davis, J.B. Ramsay, J.R. Travis, Shock initiation of solid explosives, Phys. Fluids 4 (4) (1961) 511–521.
- [60] G.I. Kanel', Kinetics of the decomposition of cast TNT in shock waves, Combust. Explos. Shock Waves 14 (1) (1978) 92–95.
- [61] YuM. Belinets, A.N. Dremmin, G.I. Kanel', Kinetics of pressed-TNT decomposition behind a shock front, Combust. Explos. Shock Waves 14 (3) (1978) 361–365.
- [62] L. Du, S. Jin, Z. Liu, L. Li, M. Wang, P. Nie, J. Wang, Shock initiation investigation of a pressed trinitrotoluene explosive, Propellants, Explos. Pyrotech. 46 (11) (2021) 1717–1722.
- [63] I.F. Kobylkin, Calculation of the critical detonation diameter of explosive charges using data on their shock-wave initiation, Combust. Explos. Shock Waves 42 (2) (2006) 223–226.
- [64] I.F. Kobylkin, Relation between the critical detonation diameter of explosive charges with characteristics of their shock-wave sensitivity, Combust. Explos. Shock Waves 45 (3) (2009) 326–330.
- [65] I.F. Kobylkin, Critical detonation diameter of industrial explosive charges: effect of the casing, Combust. Explos. Shock Waves 47 (1) (2011) 96–102.
- [66] N.P. Satonkina, D.A. Medvedev, On the kinetics of chemical reactions at the detonation of organic high explosives, Phys. Fluids 34 (2022), 087113.